Cold Regions Science and Technology 109 (2015) 9–17

Contents lists available at ScienceDirect

Cold Regions Science and Technology

journal homepage: www.elsevier.com/locate/coldregions

Detection and quantification of oil under sea ice: The view from below

J.P. Wilkinson [a,*], T. Boyd [b,1], B. Hagen [b], T. Maksym [c], S. Pegau [d], C. Roman [e], H. Singh [c], L. Zabilansky [f]

[a] British Antarctic Survey, UK
[b] Scottish Association for Marine Science, UK
[c] Woods Hole Oceanographic Institution, USA
[d] Oil Spill Recovery Institute, USA
[e] University of Rhode Island, USA
[f] Cold Region Research Laboratory, USA

ARTICLE INFO

Article history:
Received 30 September 2013
Accepted 14 August 2014
Available online 21 August 2014

Keywords:
Arctic
Oil spill
Sea ice
Oil detection
Sonar
Camera

ABSTRACT

Traditional measures for detecting oil spills in the open-ocean are both difficult to apply and less effective in ice-covered seas. In view of the increasing levels of commercial activity in the Arctic, there is a growing gap between the potential need to respond to an oil spill in Arctic ice-covered waters and the capability to do so. In particular, there is no robust operational capability to remotely locate oil spilt under or encapsulated within sea ice. To date, most research approaches the problem from on or above the sea ice, and thus they suffer from the need to 'see' through the ice and overlying snow. Here we present results from a large-scale tank experiment which demonstrate the detection of oil beneath sea ice, and the quantification of the oil layer thickness is achievable through the combined use of an upward-looking camera and sonar deployed in the water column below a covering of sea ice. This approach using acoustic and visible measurements from below is simple and effective, and potentially transformative with respect to the operational response to oil spills in the Arctic marine environment. These results open up a new direction of research into oil detection in ice-covered seas, as well as describing a new and important role for underwater vehicles as platforms for oil-detecting sensors under Arctic sea ice.

1. Introduction

The nexus of the reduction of Arctic sea ice, large untapped reserves of oil and gas within the Arctic basin, increasingly competitive Arctic shipping routes, and increasing demand for tourism have increased the need to develop improved techniques to combat potential oil spills in ice-covered waters. This is particularly important in regions subjected to a combination of enhanced sea ice retreat and human activity, such as the Alaskan outer continental shelf where current methods of oil spill response would face increased logistical and technical barriers (National Research Council, 2014). Of specific concern is the possibility of an oil spill occurring within the sea ice cover, with oil trapped beneath, or possibly encapsulated within, the ice. Despite decades of research by governmental organisations, academia and industry, the remote detection of oil under sea ice remains a challenge (Holland-Bartels and Pierce, 2011; National Research Council, 2014, PEW, 2010). Most currently applied sensing methods are deployed from on, or above, the ice surface, and thus there is a requirement that the sensor must 'see' through the sea ice and any overlying snow cover to infer the presence or absence of oil. Furthermore, most surface-based systems are impractical for deployment on young ice, deformed ice, or in the discontinuous ice conditions found within the marginal ice zone (MIZ).

In contrast, oil detection using upward-looking instrumentation from below the sea ice (mounted on underwater vehicles) avoids many of the difficulties of surface-based and airborne techniques. Unmanned underwater vehicles (UUVs) are now capable of routine under ice operation (e.g. Wadhams et al., 2004; Wadhams et al., 2006; Sohn et al., 2008; Jenkins et al., 2010; Williams et al., 2013). With appropriate sensors mounted on an UUV, mapping of oil spilt beneath the ice is now feasible. Advantages of this approach include:

(a) *Independence from weather and sea ice conditions*: UUVs have the potential to operate largely independent of ice thickness, roughness, and other physical properties in a generally quiescent ocean environment free of the effects of weather that may impede an on ice or airborne survey.
(b) *Unimpeded view of the oil:* Most importantly, for oil located below the ice, there is a direct view of the oil from the vehicle. This not only makes detection simpler for many sensors, but it also allows the use of some sensors that cannot be used from above the ice.

* Corresponding author at: British Antarctic Survey, High Cross Madingley Road, CAMBRIDGE, CB3 0ET, United Kingdom. Tel.: +44 (0)1223 221400; Fax: +44 (0)1223 362616.
E-mail address: jpw28@bas.ac.uk (J.P. Wilkinson).
[1] We dedicate this manuscript to the memory of Tim Boyd who tragically died during its preparation.

http://dx.doi.org/10.1016/j.coldregions.2014.08.004

Previous experimental releases of oil underneath sea ice revealed that oil is highly mobile and spreads along the bottom of an ice sheet as a gravity current, preferentially flowing towards regions of thinner ice and accumulating in interconnected depressions under the ice as it spreads (Fingas and Hollebone, 2003; Izumiyama et al., 2002; Wadhams, 1980; Yapa and Weerasuriya, 1997). A numerical model incorporating a regional distribution of ice-bottom morphology (i.e. the heterogeneous, natural distribution of ice thickness) revealed that the oil distribution in contaminated areas will be heterogeneous; some areas will have a light covering of oil whilst others (e.g. hollows) will experience ponding (Wilkinson et al., 2007). An oil detection system should then be able to both determine the presence of oil under sea ice, as well as the thickness of the oil.

Due to high contrast between oil (black) and the ice bottom (white) digital imaging is potentially a simple and highly effective method for mapping the extent of oil located under ice. It has the advantage of being a well-established technology for underwater surveys with a wide variety of systems and image processing and classification software available. It's two-dimensional data allows straightforward delineation of the extent of a spill, although the high data volume may limit real-time data transmission. In most instances, it easy for a human operator to interpret, although variable light levels and turbid water may complicate discrimination of oil from bare ice.

Active acoustics offers the possibility of detecting not only the oil, but also its thickness. Sea ice is a relatively strong reflector of sound because of the acoustic impedance contrast between seawater and the ice bottom. The effectiveness of the ice/water interface in reflecting incoming acoustic energy has enabled the use of sonars to detect and map the underside of sea ice (Wadhams et al., 2006), and has contributed to early awareness of the changing climate of Arctic sea ice (Rothrock et al., 1999). The somewhat weaker scattering from oil due to the smaller acoustic impedance contrast between oil and seawater may be exploited to detect the presence or absence of oil under sea ice.

When the oil is pooled beneath the ice, it forms a multilayer system of seawater, oil, and ice. By detecting discrete reflections from each interface, the thickness of the oil layer may be determined, which when the extent is also mapped (e.g. by sonar or digital imagery), the volume of oil can also be determined.

In this paper we present results from a sea ice tank experiment to evaluate the potential for upward-looking optical and acoustic sensors suitable for deployment on an UUV to detect the presence and thickness of oil spilled under sea ice.

2. Methods

Oil spill experiments under sea ice were carried out at the US Army Cold Regions Research and Engineering Laboratory (CRREL) in Hanover, New Hampshire. Sea ice was grown in the outdoor Geophysical Research Facility tank (18.25 m long, 6.7 m wide, and 2 m deep) over the 2011–12 winter period leading up to experiments on January, 18–20, 2012. Hollows of dimensions of about 2.4 m by 1.2 m (in the along- and across-tank directions, respectively) were produced in the underside of the ice by placing insulating boards over the upper surface of the growing ice so that these areas were slightly thinner than the surrounding ice. Alaska North Slope (ANS) crude oil was injected into these pockets, where it pooled. A sensor suite including cameras, sonars, and a laser system was mounted on a trolley travelling on rails along the tank bottom (Fig. 1).

The results presented here are from observations of a sequence of two oil injections into a single ice hollow using the sonar and camera systems. The experimental sequence was as follows:

(1) The ice underside was mapped (via sonar) to clearly distinguish between the hollows and flat regions,
(2) The trolley was parked under the central region of the hollow,
(3) Oil was injected into the hollow and its spread was observed, and
(4) A second measure of oil was injected into the same hollow.

Additional observations were made to map the spill by moving the trolley beneath the hollow. These observations are qualitatively similar to the stationary measurements but of lower quality as jittering of the trolley as it moved along the rails affected the sonar signal, and are thus not presented here. The characteristics of the experiment are summarised in Table 1.

2.1. Delivery of oil

The oil was delivered from a 20 litre pressurised canister-based system mounted on the surface of the ice (Fig. 2). An air compressor forced oil from the canister through a hose that ran through a PVC pipe frozen into the ice at the edge of the hollow and then to the base of the ice in the hollow. This allowed accurate determination of the volume of oil released whilst ensuring stable delivery of the oil to the ice underside and preventing spread of the oil beyond the edge of the hollow of flow back out of the hole and onto the ice. Details of the experimental setup are given in Table 1.

2.2. Instrumentation

2.2.1. Camera system

Two upward-looking Prosilica high dynamic range cameras (one colour, and one black and white) were mounted on the sensor trolley to provide overlapping views of the ice bottom. These cameras are designed for extremely low-contrast applications typical of underwater (and under ice) applications. These colour-calibrated cameras have a 12-bit dynamic range with a resolution of 1380 × 1024 pixels and a field of view (FOV) of 39.5° horizontally and 30.5° vertically.

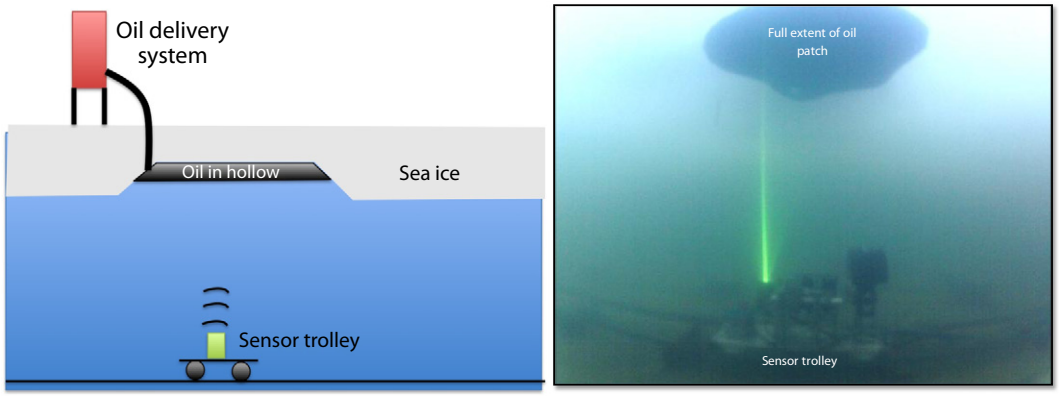

Fig. 1. Left: Cartoon showing the experimental layout. The sensor trolley was located on tracks at the tank bottom. All sensors looked up towards the oil that was located just over a metre above. Right: Under sea ice oil slick and sensor trolley as viewed from the side using an underwater, wide angle "Go-Pro" camera. The green light is from a sheet laser system that accompanied the sonar and cameras on the trolley.

Table 1
Parameters of the experiment conducted on 19 January 2012.

Characteristic	Value	Characteristic	Value
Air temperature	−6.7 °C	Level ice thickness (measured)	0.5 m
Crude oil type	Alaska North Slope (ANS Crude)	Water temperature: (measured)	−1.3 °C
Oil temperature	−4.2 °C	Water depth (approximate)	2 m
Times of oil injection	First: ~15:10 EST, Second: ~17:00 EST	Sonar head distance to level ice (measured)	1.08 m
Dimensions of hollow	2.4 m × 1.2 m	Sound speed (inferred)	1430 m s^{-1}
Depth of hollow (measured)	0.10 m	Water salinity (inferred)[a]	25 psu
		Water salinity (measured)	33 psu

[a] The calculated water salinity of 25 psu was based on the measured water temperature of −1.3 (freezing point) and not the 33 psu as measured at the bottom of the tank. As the salinity (bottom) and water temperature (top) were measured at different depths this discrepancy could be due to haline stratification within the water column. The origin of the halocline could be from incomplete mixing of the water column when the salt was added and further enhanced by the additional release of brine during sea ice formation.

With the cameras located at about 1.18 m from the underside of the sea ice hollow, the FOV covers 0.5185 m^2 (0.85 m by 0.61 m) of ice bottom. The cameras were set to take a photograph every 2 s. Continuous visual detection provided both visual confirmation of the presence or absence of oil and the spreading rate.

2.2.2. Sonar altimeter

A 1.1 MHz echo sounder (Marine Electronics Ltd: Model 11001 Multi-Return Altimeter) with a 1.6° (+/−3 dB) conical beam was used. At a distance from the ice bottom of 1.18 m from the sonar head, the insonified footprint was 3.3 cm in diameter (8.5 cm^2 in area). The sonar pulse length was 10 μs, corresponding to a pulse length of 0.014 m for a sound speed of 1430 m s^{-1}. The return signal was subsampled into 1 μs bins. The ping rate was set to yield an independent profile every 1 s, however this rate drifted slightly and the results shown here have been shifted to the nearest whole second. This high frequency (1.1 MHz) provided excellent resolution, so that thin oil slicks might be detected, however, in a real application this frequency (1.1 MHz) would limit the range to typically <30 m from the ice bottom, so the host vehicle would need to be relatively close to the underside of the sea ice.

The distance between the sonar head to ice bottom was measured to be 1.08 ± 0.01 m. For an ~1 μs error for the travel time recorded by the sonar, the sound speed is estimated to be in the range of 1417–1443 m s^{-1}. We have used the central value of 1430 m s^{-1} (Table 1).

Fig. 2. Photograph showing the filling of the pressurised oil delivery system. This system allowed oil to be deployed efficiently and effectively as well as constraining the oil to the experimental hollow under the sea ice. No evidence of oil spreading beyond the hollow was seen.

3. Results

3.1. Visual detection of oil

After the injection of oil, its flow along the underside of the hollow was clearly visible with both upward-looking high dynamic range camera systems (Fig. 3). During daylight no additional illumination was needed to detect the oil, which is not surprising given the relatively thin ice (0.5 m) and lack of snow cover. At night a laser system on the trolley (Fig. 1) provided enough illumination for the high-dynamic range cameras to clearly differentiate between oil and ice (Fig. 4). In regions of high snow loading (snow is very efficient at attenuating sunlight) or during the polar night artificial lighting may be necessary. Further experiments are needed in order to determine the limits of detection under differing scenarios, including deep snow, longer range (i.e. 10–20 m), or for cases in which oil is encapsulated by ice forming beneath it.

By examining the sequence of images as the oil spread within the hollow, the spreading rate can also be determined. Understanding of the spreading behaviour of the oil is important for accurate modelling of the dispersal of an oil spill under sea ice (Wilkinson et al., 2007). Using a sequence of ~150 sequential images over the 5 min after the oil was first seen by the camera, we used a simple, automated, grey-scale thresholding method to discriminate between ice and oil in each photograph. The areal spreading rate was determined by calculating the change in area between consecutive images from the number of pixels classified as oil. Over the 5 min, the spreading rate reduced from an initial 7 cm^2/s, to a near constant rate of ~9 cm^2/s. This rapid stabilisation of the spreading rate to a constant rate is consistent with prior observations and theoretical predictions (e.g. Izumiyama and Kono, 2002; Yapa and Chowdhury, 1990) with constant oil discharge, suggesting that the observed spread was still driven by the oil delivery system at this stage and not purely gravity driven.

3.1.1. Discussion of camera results

These results show that an upward-looking camera system can be a very effective tool for detecting oil on the bottom of the ice and monitoring the boundaries of the slick as it spreads. The contrast between ice and oil simplifies the classification problem and therefore a human operator can quickly and easily verify automated classification and oil detection techniques. Like all optical techniques, its efficacy will be impacted by changes in ocean clarity and the variable light levels that may be found under sea ice. These factors, often present under a variable ice cover, may be difficult in some circumstances. In such cases, additional information from other sensors will be valuable to confirm the presence or absence of oil.

Whilst visual techniques are simplest for an untrained operator to quickly interpret, they provide only a two-dimensional map of the oil spill and do not provide any quantitative information on the oil thickness. Oil will pool in pockets of undulating relief on the bottom of the ice cover and in thinner ice areas. To best quantify the volume of oil

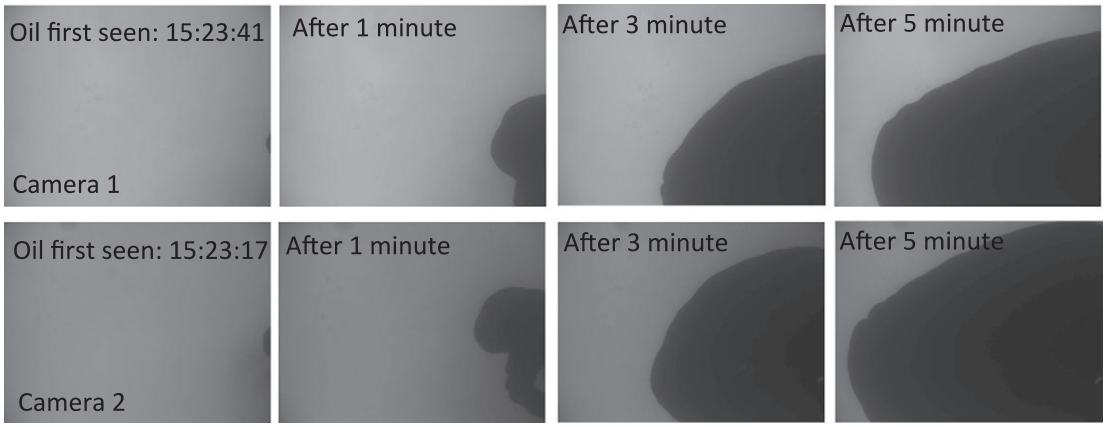

Fig. 3. Selection of photos showing the flow of oil within the hollow over the first 5 min. The top time-series is from camera 1 and the bottom series is from camera 2. As the cameras were located at different positions on the trolley their field of view is slightly different. For example the oil entered the field of view of camera 2 about 24 s before camera 1. Field of view for each photograph is 0.5185 m^2.

knowledge of the oil thickness needs to be obtained simultaneously with the extent of the oil discharge under the ice. This may be determinable with acoustic methods.

3.2. Acoustic detection of oil

The relative amount of acoustic energy reflected from an interface for a wave that hits a boundary at normal incidence is dependent on the relative acoustic impedances in the two media:

$$R_{12} = \left(\frac{z_2 - z_1}{z_2 + z_1}\right) \quad (1)$$

where R is the amplitude reflection coefficient, z_1 and z_2 are the impedances of the first and second media, and $z_i = \rho_i * c_i$ is the acoustic impedance of the two media of density ρ_i and sound speed c_i respectively. Using typical acoustic impedances for the different media encountered during the experiment (i.e., sea ice, seawater, air and oil, Table 2), the reflection coefficients of various interfaces can be estimated (Table 3). In Table 2, the impedance of sea ice is calculated using a bulk density of 950 kg m^{-3} (for a brine content of 30% in the skeletal layer), and a sounds speed of 1700 m s^{-1} for the skeletal layer (Garrison et al., 1991).

The reflection coefficient from sea ice varies considerably due to the complex morphology of the skeletal layer of dendrites at the ice/ocean interface (Stanton et al., 1986), and variations in sound speed in the reflecting basal layer (Garrison et al., 1991). Laboratory and field measurements show that the structure of the ice underside has a strong influence on the reflection coefficient, spanning the range 0.04–0.27 (Jezek et al., 1990). For thin ice, where a pronounced skeletal layer exists, the reflection coefficient will be at the low end of this range, and comparable to the reflection from an oil–water interface. But for thicker (or older) ice the skeletal layer is often less developed, and we might expect a much stronger reflection from the bottom of the ice than from a crude oil layer. This appears to be the case in our experiments (Fig. 5), where the reflection from the ice/water interface was much stronger than the initial reflection from the oil. As the reflected signal from the ice was saturated and the sonar uncalibrated, we cannot accurately determine the reflection coefficients. However, the observed scattering is qualitatively consistent with a more strong scattering ice bottom.

The lower reflectance of an oil/seawater interface vs. an oil/ice interface is a desirable property for detecting oil pooled beneath the ice, particularly for thin layers. These observed differences in scattering properties may be exploitable to discriminate ice from oil (especially if supplemented by digital imagery). However, the wide range of scattering characteristics for different ice types suggests that the differences in scattering may not be consistent. In this case, the ability to detect multiple scattering interfaces as seen in Fig. 5 is likely to be more useful.

3.2.1. Detection of oil thickness

Once the oil was injected, its flow along the underside of the ice was clearly documented by the upward-looking camera system that was mounted on the trolley (Fig. 3). The oil flowing over the region insonified by the sonar is initially very thin, however within a few tens of seconds it reached an apparent thickness of about 0.01 m. For the next 6 min the sonar detected an oil thickness increase of about 0.02 m (Fig. 5). Although with a pulse length of 10 μs the vertical resolution is ~0.014 m, the reflection from the leading edge of the pulse was clearly seen, so that changes in oil thickness as small as 0.0014 (the binning interval used) were possible. Because of the pulse width,

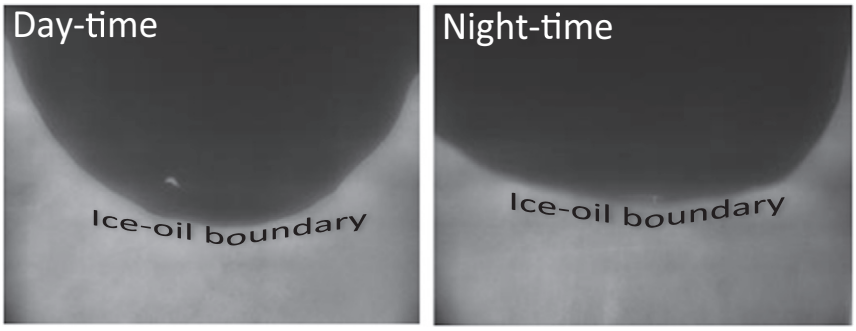

Fig. 4. Photograph of the underside of the hollow taken during daylight hours (left) and at night (right). The illumination for the night-time photograph was provided by a sheet laser system installed on the instrument trolley.

Table 2
Acoustic impedances for materials encountered in the experiment.

Material	Impedance (MRayl)
Air (P = 1 bar, T = 20 °C)	4×10^{-4}
Fresh ice	3.5
Sea ice (after Garrison et al., 1991)	1.62
Seawater (S = 32, T = −1.5 °C)	1.48
Crude oil (Jones, 2010)	1.3

1 Mrayl = 10^6 kg m^{-2} s^{-1}.

discrimination of multiple interfaces spaced more closely than half the pulse length (or ~0.007 m in this case) would be more difficult. If the interface is irregular, due to either thickness variations within the sonar footprint or broadening of the transmitted pulse as it interacts with the porous skeletal layer (up to 1 cm or more in thickness) found at the base of growing ice, the minimum separation may be significantly larger.

Small variations in apparent thickness were detected during this time. The cause of these variations is unclear, but is most likely due to variations in the flow of oil due to interactions between the flowing oil and small-scale roughness of the ice bottom.

The injection process took around 10 min, and for the next 30 min the thickness of the oil layer in the hollow increased slowly to about 0.03 m, after which the oil thickness did not increase, suggesting that the oil reached its maximum extent within the hollow and thereafter the slick remained motionless. Interestingly, the diminishing motion within the oil slick coincided with a cleaner sonar return from within the oil layer, and an increase in the strength of the return from the oil/water interface (see Fig. 6). Whilst the origin of the complex acoustic signatures before the slick became motionless is not clear, it does suggest that based on their acoustic signal it may be possible to differentiate between regions of flowing oil from those regions that are stagnant. However further work is needed as the increase in signal strength might be due to a more level oil surface — thus reflecting more energy directly back to the sonar.

A second oil injection, about 90 min after the first injection, is shown in Fig. 6. The spreading of newly injected oil deepens the oil–water interface by about a centimetre. For about 5 min after the arrival of the oil we observe a short-term increase in amplitude of the reflection from the water/oil interface. It is not clear what the reason behind these short-lived high amplitude returns from the oil–water interface is, but they could be due to ice crystals or bubbles forming on the oil surface. Just after the 100 min mark (Fig. 7) there is a sudden apparent downward movement of the ice–oil interface of ~0.015 m, accompanied by temporary reduction in the reflection strength from the oil–ice interface, followed by an increase in reflection strength. This shift appeared to be accompanied by audible bubbling through the oil hose. As there was no sustained change in position of the oil–water interface, but there was in the ice–oil interface, the most plausible explanation is an accidental injection of air through the oil line. Alternatively, it may have been a movement of the ice surface itself, accompanied by further movement of the oil.

Table 3
Theoretical acoustic reflectance for interfaces encountered in the experiment calculated using Eq. (1). *R* for seawater is based on impedance for salinity of 32 psu and temperature of −1.5 °C. *R* for oil is based on impedance for crude oil. The reflection coefficients in brackets are from measurements (Jezek et al., 1990).

Interface type	Reflection coefficient
Seawater–pure ice	0.41
Seawater–sea ice	0.045 (.04–0.27)
Seawater–crude	0.065
Crude–ice	0.11
Air–all others	0.9999

If air rose up through the oil and was trapped in a thin layer at the base of the oil, it would form a strong scattering layer beneath the ice due to the substantial oil/air acoustic impedance mismatch (Tables 2 and 3). A thin strong reflecting layer (~1 cm) would not be resolvable from the ice layer above given the similar pulse length. This may be a proxy for a spill in which gas is also beneath the ice. In this scenario, the gas may not be able to escape through the ice, creating a four layer system, i.e. ice, gas, oil and finally, seawater. However, because of the opacity of gas to sonar, it may not be possible to distinguish gas from ice without additional information. Fig. 8 shows time-sequence of acoustic profiles of returned acoustic signal amplitude from the end of Day 1 and at the beginning of Day 2, a separation of about 13 h, and 19 h after the initial release of oil. These data were recorded at the identical location as the trolley was left parked under the hollow overnight.

There are substantial changes in the acoustic profiles collected at the end of Day 1 with those from the beginning of Day 2. Whilst the location of the oil–ice interface remains constant at around 1.17 m from the sonar, the oil–water interface moved upward (i.e. the oil layer thinned), from a distance of about 1.13 m at the end of Day 1 to 1.135 m at the start of Day 2. It is unclear if this was due to continued, slow spreading of the oil within the hollow, or percolation of the oil into the porous brine network within the ice (Martin, 1979).

The most significant change was a reduction in the acoustic return amplitude from oil–ice interface and an increase from the oil–water interface. These changes are consistent with a thin layer of sea ice growing beneath the oil, encapsulating it between two layers of sea ice, i.e. changing the system from a three-layer system (water–oil–ice) to a four-layer system (water–ice–oil–ice). This layer must have been very thin — perhaps a few crystals and not even a continuous layer of ice, as this could not be clearly seen in the camera imagery. It is however consistent with the change in the strength of the reflections from each medium.

3.2.2. Minimum oil detection thickness and the impact of the pulse length

In each of the profiles of returned acoustic signal amplitude (Figs. 5 through to 8) the water/oil and oil/ice interfaces are readily discernible, both within individual traces (left panels) and as an overall pattern of evolution of contours of return amplitude (right panels). However, very thin layers are more readily identifiable in the continuous records where the time evolution can be observed as the layer thickens. As described above, the minimum practical layer separation that can be observed is equal to the pulse width (1.4 cm in this case). However, smaller separations between the water/oil and oil/ice interfaces may be detectable (e.g. when oil is initially detected in Fig. 5) when there is significant differences in the magnitude of the scattered signal from the two interfaces (as is the case here), so that the scattering from the leading edge of the pulse is discernable, even when the reflected pulses from the two interfaces overlap. Thus, the differences in the acoustic signatures of oil and ice might be useful to detect very thin oil layers. Once the scattering strength from the oil increases (Fig. 8B, possibly due to encapsulation, see below), the returned pulses from the first reflection would dominate and subsequent pulses at spacings less than the pulse width impossible would likely no longer be identifiable.

For an irregular ice underside where oil will pool to significant thickness in hollows (Norcor, 1975) the minimum detectable spacing between interfaces is less of a concern. But for oil that is dispersed beneath smooth ice, the ability of the oil to spread thinly could complicate detection.

Fig. 9 displays the acoustic amplitude returns from five separate sonar pings during the initial flow of oil over the region insonified by the sonar. These are at 10 second intervals surrounding the first appearance of the oil (from 10 s before the oil is seen by the sonar, t = −10, to 30 s after, t = 30).

The thickness of oil when first seen by the sonar (t = 0) is around 0.2 cm. This very thin oil slick may be a function of the curvature of the head of the flowing oil. After 10 s the oil reaches and maintains a

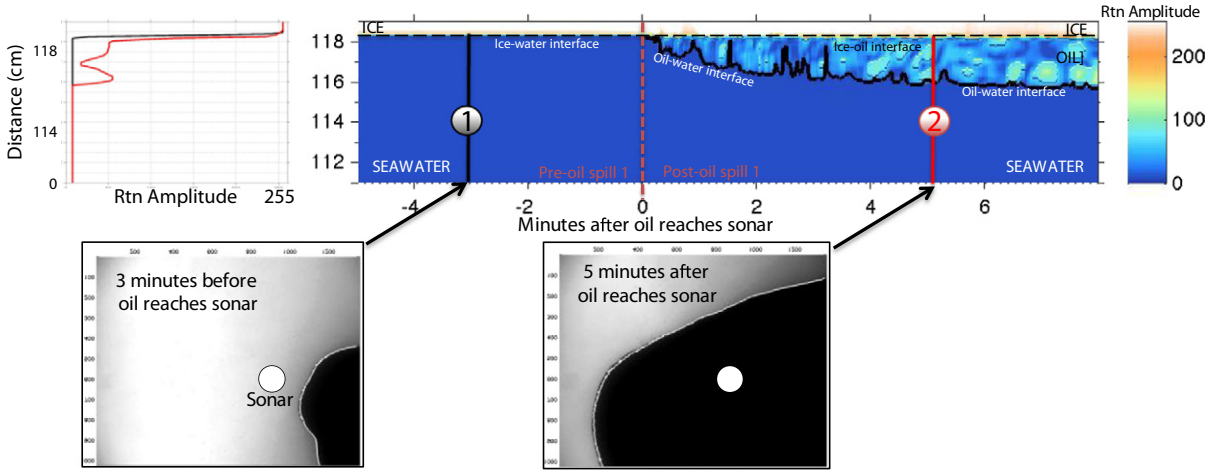

Fig. 5. Sonar and photographic data from the initial spill of oil. Distances from the sonar head (y-axis) are inferred from a two-way travel time using the appropriate sound speed for water. Top left: The return acoustic signal amplitude for profile 1 (shown by the vertical black line in the top right panel) obtained 3 min before the oil reaches the area insonified by the sonar (black line). The return acoustic signal amplitude for 5 min after the oil first passes under the sonar is shown in red (shown by the vertical red line in the top right panel). These data have been passed through a median filter of width 2 μs. Top right: Time-sequence of profiles of returned acoustic signal amplitude spanning 3 min before the oil reaches the area insonified by the sonar and 5 min after. Colours represent the intensity of the return amplitude, deep blue being low and white representing high returns. A solid black line represents the oil–water interface in the middle, whilst the horizontal dashed line represents the location of the ice interface. Vertical solid lines represent the location of the amplitude time sequence seen in the top left panel. Bottom: Photographs from the upward-looking camera showing the location of both the oil and region insonified by the sonar.

thickness of about 1.4 cm and stays around that thickness for the next 20 s. This is slightly thicker than the 0.5–1 cm thickness seen in previous oil under ice experiments (Dickins et al., 1975; Keevil and Ramseier, 1975), possibly because the oil was constrained by the dimensions of the hollow and was not able to spread out uninhibited along the under-ice surface. Importantly, the shape of the returned profile is changed due to the lower reflected signal strength from the oil versus the ice interface even for very thin oil thicknesses. This suggests that differences in the scattering characteristics between sea ice and oil could be exploited to detect thin oil slicks that are present on the underside of sea ice. To better determine if this is possible in a real-world application where ice conditions are unlikely to be uniform requires further investigation of the acoustic scattering characteristics of multiple types of sea ice and oil.

The finite footprint of all sonars due to beam spreading, and beam side-lobes will cause signal clutter as it interacts with an irregular ice underside, such that the returned signal will exhibit pulse broadening. By broadening the returned pulse, the minimum spacing that can be resolved between interfaces will increase in a way dependent on the sonar beam pattern, distance of the sonar from the ice underside and the morphology of the ice bottom. Multiple reflections from the interfaces will further complicate the returned signal. Further experiments to characterise the acoustic response of thin layers of oil under ice, and in more realistic conditions are needed to determine the minimum practical thickness of an oil layer detectable with sonar.

3.2.3. Variability in sound speed: apparent shift in interface range

The distances of the water/ice and oil/ice interfaces from the sonar (Figs. 5–8) are derived using a single sound speed for the entire propagation distance, which is not appropriate after the introduction of the layer of oil. Prior to introduction of oil, the acoustic range to the water/ice interface is consistent with the measured distance to the interface (1.18 m). After the introduction of the oil, the apparent distance to the oil/ice interface is slightly less (~0.8 mm), due to the more rapid sound propagation across the oil layer (Fig. 9). For a calculated oil thickness of 2.75 cm at an assumed sound speed of 1430 m s^{-1}, we get a corrected oil sound speed of 1470 m s^{-1}. For an assumed density of 910 kg m^{-3} for Alaska North Slope blend crude oil (Jones, 2010), this results in an impedance of 1.33 MRayl which compares well with the prior estimate of 1.3 MRayl (Jones, 2010, and Table 2).

3.2.4. Detection of flowing oil and non-flowing oil

When the oil layer is in motion and the interface at the leading edge of the slick is disturbed, variation in returned signal strength is observed. As the oil layer spreads as a gravity current, either irregularities in the delivery rate of the oil or drag across the interface likely leads to undulations in the oil thickness in the first few minutes of oil being seen by the sonar (Fig. 5). These undulations may scatter some acoustic energy away from the sonar, thus contributing to a reduced received signal strength relative to later in the time series. This variability is

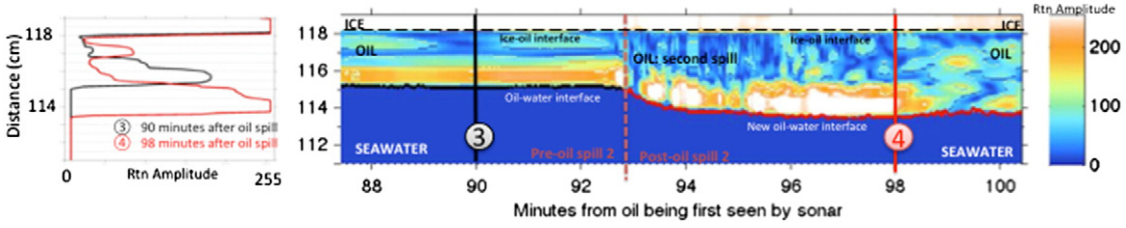

Fig. 6. Echograms during the second oil release. Left: The black line is the acoustic amplitude profile 3 min before the second oil injection reaches the area insonified by the sonar. The return profile 5 min after the oil first passes under the sonar is shown in red. A median filter of width 2 μs was used to reduce the noise in these profiles. Right: Time-sequence of returned acoustic amplitude profiles spanning 3 min before the oil reaches the area insonified by the sonar and 5 min after. Colours represent the intensity of the return amplitude, deep blue being low and white representing high amplitude (arbitrary scale). The solid black or red line represents the oil–water interface, whilst the horizontal dashed line represents the location of the ice–oil interface. Vertical solid lines show the location of the acoustic profiles shown in the left panel.

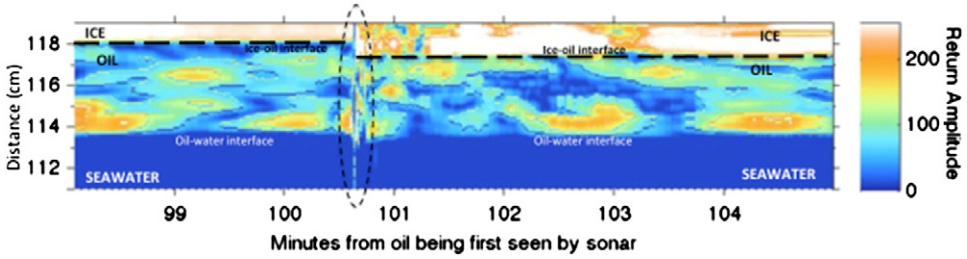

Fig. 7. Possible evidence of air located between the oil–ice interface. Within the circled area an apparent shift in the oil–ice interface (black dotted line) of about 0.015–0.02 m is seen.

possibly enhanced by turbulent motion of small inclusions of water. Other plausible explanations include ice crystallisation as the cold oil hits supercooled water or small air bubbles or other impurities within the oil.

The difference between flowing and motionless oil can be clearly seen in Fig. 6. Immediately following the second injection of oil (Fig. 6), small scale variability returns throughout the full depth range of the oil layer, which diminishes after about 25 min (not shown).

3.2.5. Oil infiltration into sea ice and encapsulation

After the underside of the sea ice has been in contact with the oil for approximately 18 h we see an apparent reduction in the thickness of the oil of ~0.5 cm, accompanied by a substantial increase in the reflectivity of the oil–water interface, and a reduction in the received reflected signal from the base of the ice (see Fig. 8).

A possible reason for the reduction in oil layer thickness is the infiltration of oil into the skeletal layer or inside the brine channels themselves. Evaluation of these possible sources of variability is an important issue, especially for thin films under sea ice as they may be incorporated into the skeletal layer of the growing sea ice, thus making detection more difficult, or for warm ice, where the oil may percolate up through the ice. Field and laboratory tests show that encapsulated oil is released in the spring/summer melt period by either vertical migration of oil through the ice and its brine channel system or through the ablation/melt of the ice surface downwards (Fingas and Hollebone, 2003). If oil entrained in the skeletal layer can indeed be detected acoustically, this may be a useful means to further study the interaction oil with sea ice.

If a spill occurs when the ice is actively growing then sea ice will form beneath the oil, encapsulating the oil within the ice matrix (NORCOR, 1975). The strong increase in acoustic scattering from the base of the ice (Fig. 8) is likely due to the initiation of encapsulation. The increase in the scattered energy received from the base of the oil layer is accompanied by a broadening of the signal across the interface, consistent with scattering from both the new ice layer and the oil beyond. This is accompanied by an expected decrease in scattered energy received from the original ice bottom as less of the acoustic energy is transmitted across the now more reflective interface at the base of the oil layer. Further dedicated tests are needed to quantity the detection

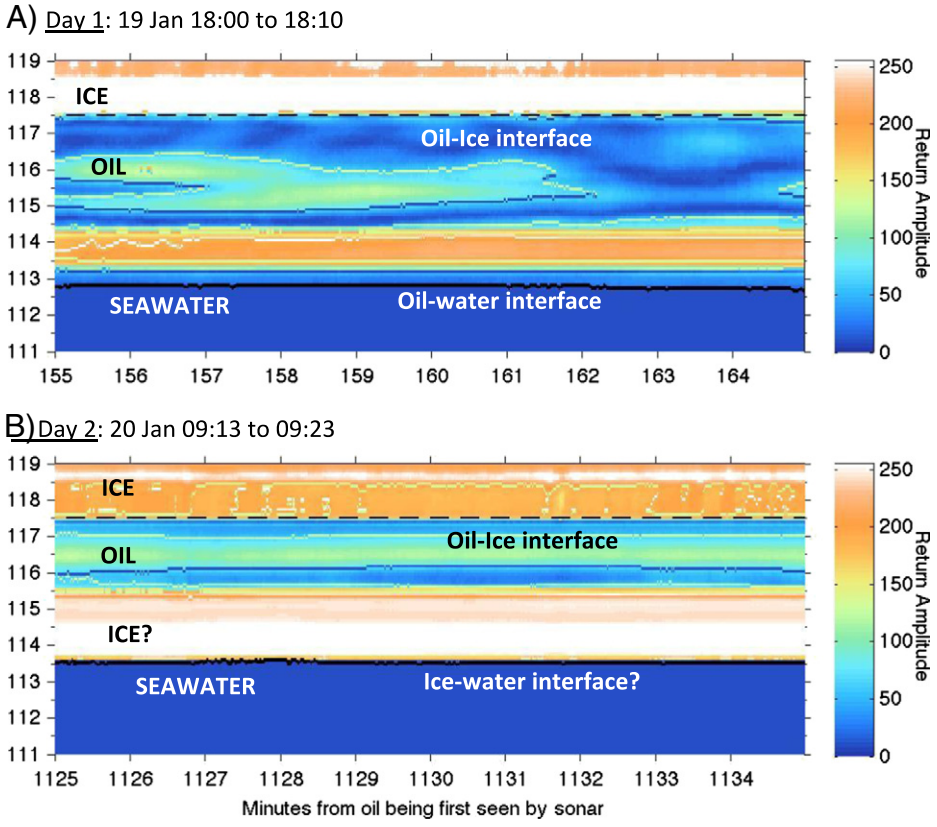

Fig. 8. Profiles of returned acoustic signal amplitude from the end of Day 1 and at the beginning of Day 2, a separation of about 13 h. Processing is as described in Fig. 5. The increase in amplitude of the acoustic return from the oil–water interface suggests that the oil may have been encapsulated by a thin layer of sea ice growing beneath the oil. The apparent vertical extent of the interface and the oil/ice interface is due to the finite length of the transmitted acoustic pulse (1.43 cm) interacting with the interface, and does not reflect the thickness of this ice, which is presumed to be only millimetres thick.

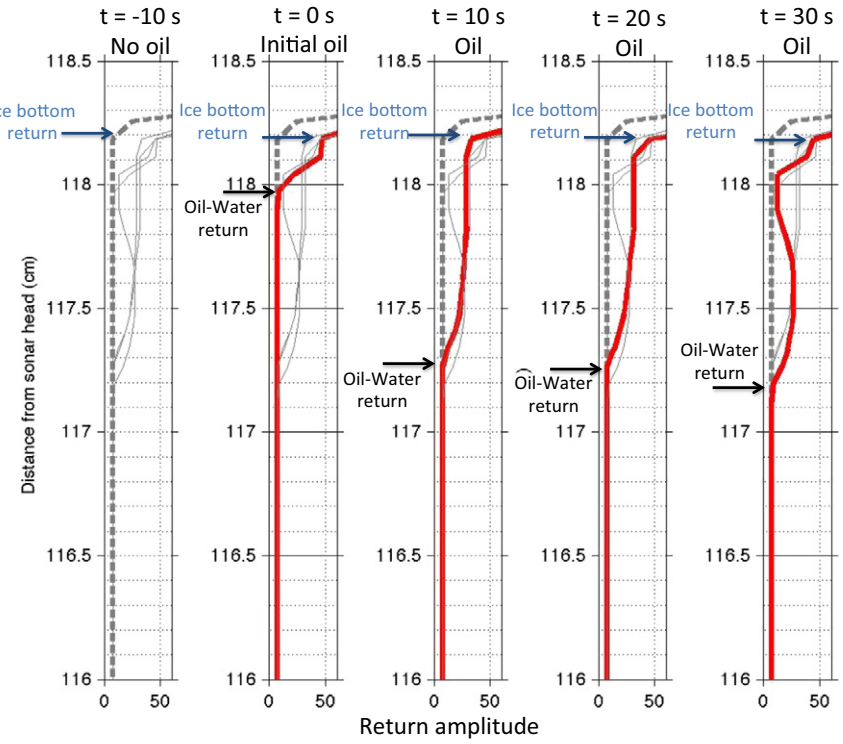

Fig. 9. Acoustic amplitude profiles returned from five separate sonar pings during the initial flow of oil over the region insonified by the sonar. When the estimated oil thickness is only 2 mm (second profile from left), a change in the acoustic profile is detectable, demonstrating, in principle, that very thin oil layers may be resolved based on the shape of the returned pulse waveform.

of oil encapsulated in sea ice through acoustic (and visible) means for greater depths of encapsulation.

4. Discussion and conclusions

In order to respond to an oil spill under sea ice, it is desirable to know where the oil is and its thickness so that the volume may be determined. These results demonstrate that acoustic and visual measurements from below can quantify the area and thickness of a layer crude oil directly beneath sea ice. Importantly, it may also be possible to detect oil that has been encapsulated by the growing sea ice by acoustic methods.

In these experiments, a difference in scattering strength was seen between the underside of clean sea ice and oil, although the latter increased with time, possibly due to ice forming beneath the oil. However, it is known that the scattering characteristics of sea ice depend strongly on thickness and structure (Jezek et al., 1990; Stanton et al., 1986; Williams et al., 1992) and sonar frequency (Garrison et al., 1991), which may make discrimination difficult based on scattering statistics. The detection of the oil–ice interface could be more complicated because the presence of oil may modify the acoustic signature of the ice. As oil flows under growing sea ice, it can affect the porous skeletal layer in the bottom several centimetres of the ice either through melting or by buoyant percolation into the porous brine network (Martin, 1979).

Detection with sonar is most readily achieved by exploiting the distinctive, multiple returns due to reflections from both the oil–water and oil–ice interfaces, so that not only can the presence of oil be detected, but also its thickness, even for layers a few centimetres or less in thickness. In this case, identification of the interfaces was straightforward and required minimal processing of the acoustic data, which is an important feature for future operational use.

There are a number of potential complexities that may complicate detection in real-world conditions, including irregular ice morphology (particularly in broken ice, ridged ice, and rubble), encapsulation of the oil within thicker ice layers (where penetration of the sonar signal into the ice becomes an issue), and percolation of the oil into the sea ice. In summer, under ice melt ponds, which introduce low salinity melt water beneath the ice, may have an acoustic signature similar to a pool of oil beneath the ice. The base of these ponds can freeze, creating false bottoms on the underside of the ponds, which will mimic encapsulated oil.

The potential for false positive detection of oil in such circumstances highlights the need for a multi-sensor approach to oil detection under ice. The large visible contrast between ice and oil in images simplifies the classification process; when coupled with a sonar system, this is likely to greatly reduce any ambiguity in the interpretation of the sonar signal. However, as with all optical methods, camera-based oil detection is sensitive to variability in the optical properties of the overlaying water column, whether natural or spill-related (Moline et al., 2012). Additional laboratory tests are needed to quantify the effects of these and other ice conditions on the returned acoustic signal.

In real world conditions, because of the presence of sea ice keels (highly heterogeneous fractured sea ice) it is likely that the UUV platform will need to stand-off the ice bottom by a few tens of metres, therefore the range of the sonar must be taken into consideration. The 1.1 MHz frequency used here would give a useful range of up to about 30 m. Lower frequency sonars would permit surveys at greater distances, but at the expense of reduced range resolution. Because the sonar footprint increases with distance to the target, the ice roughness scales within that footprint will affect the scattering characteristics and the ability to resolve thin layers.

For a camera system, a stand-off distance of a few tens of metres could significantly impact the quality of the images produced, although this will be very much dependent on the ambient light conditions Under low-light conditions a strobe may be required to illuminate the ice bottom. This is a standard technique used on UUVs to provide imagery in low-light and full-darkness conditions i.e. deep sea.

Although these laboratory observations were conducted for the simplest sea ice conditions (flat, unbroken ice in freezing conditions), our findings demonstrate a proof of concept for the acoustic detection

(with or without cameras) of the layered structure associated with an oil spill under sea ice from below. These results provide the first demonstration that detecting of oil from beneath sea ice, where the need to "see" through the ice is reduced or obviated entirely, can be achieved.

The capabilities of unmanned underwater vehicles and remotely operated vehicles for under ice operations are rapidly improving and the results shown here have wider implications for the development of operational systems for oil spill detection in ice-covered waters. These results provide the first proof of concept for use of sonar and camera systems (possibly in conjunction with other sensors) on UUVs for the detection of oil under sea ice. Further experimental testing of these sensor systems and investment in development of UUV capabilities under ice is needed to evolve these techniques towards an effective operational solution to the long-standing problem of detection of oil under sea ice.

Acknowledgements

This work was funded through a competitive grant for the detection of oil under ice obtained from Prince William Sound Oil Spill Recovery Institute (OSRI) (11-10-09). Additional funding/resources was obtained through the EU FP7 funded ACCESS programme (Grant Agreement n°. 265863).

References

Dickins, D., Overall, J., Brown, R., 1975. Beaufort Sea Project Tech. Rept. 27. Inst. of Ocean Sciences, Victoria B.C.

Fingas, M.F., Hollebone, B.P., 2003. Review of behaviour of oil in freezing environments. Mar. Pollut. Bull. 47 (9–12), 333–340.

Garrison, G.R., Francois, R.E., Wen, T., 1991. Acoustic refections form arctic ice at 15–300 khz. J. Acoust. Soc. Am. 90 (2), 973–984. http://dx.doi.org/10.1121/1.401965.

Holland-Bartels, B. Pierce, 2011. An Evaluation of the Science Needs to Inform Decisions on Outer Continental Shelf Energy Development in the Chukchi and Beaufort Seas, (Alaska, U.S. Geological Survey Circular 1370, 2011).

Izumiyama, K., Kono, A., 2002. Experimental study of spreading oil under ice covers. Proc. Int. Offshore and Polar Engineering Conf (Japan, May 26–31).

Jenkins, A., Dutrieux, P., Jacobs, S.S., McPhail, S.D., Perrett, J.R., Webb, A.T., White, D., 2010. Observations beneath Pine Island Glacier in West Antarctica and implications for its retreat. Nat. Geosci. 3, 468–472 (http://dx.doi.org/10.1038/ngeo890).

Jezek, T.K. Stanton, Gow, A.J., Lange, M.A., 1990. Influence of environmental conditions on acoustical properties of sea ice. J. Acoust. Soc. Am. 88 (4), 1903–1912. http://dx.doi.org/10.1121/1.400213.

Jones, J.C., 2010. Hydrocarbons — Physical Properties and Their Relevance to Utilisation. J. C. Jones & Ventus Publishing ApS. p111, (http://bookboon.com/en/hydrocarbons-ebook).

Keevil, B.E., Ramseier, R., 1975. Proceedings of the 1975 Conference on Prevention and Control of Oil Pollution. American Petroleum Institute, USA, pp. 497–501.

Martin, S., 1979. A field study of brine drainage and oil entrainment in first-year sea ice. J. Glaciol. 22, 473–502.

Moline, M.A., Robbins, I., Zelenke, B., Pegau, W.S., Wijesekera, H., 2012. Evaluation of bio-optical inversion of spectral irradiance measured from an autonomous underwater vehicle. J. Geophys. Res. 117. http://dx.doi.org/10.1029/2011JC007352.

NORCOR, Engineering and Research Ltd, 1975. The interaction of crude oil with Arctic sea ice. Beaufort Sea Technical Report, No. 27, Beaufort Sea Project. Department of the Environment, Victoria, BC, p. 201.

PEW, 2010. Oil Spill Prevention and Response in the U.S. Arctic Ocean: Unexamined Risks, Unacceptable Consequences, (November 2010. 136p).

National Research Council, 2014. Responding to Oil Spills in the U.S. Arctic Marine Environment. The National Academies Press, Washington, DC (250 pp).

Rothrock, D.A., Yu, Y., Maykut, G.A., 1999. Thinning of the Arctic sea-ice cover. Geophys. Res. Lett. 26 (23), 3469–3472.

Sohn, R.A., et al., 2008. Explosive volcanism on the ultraslow-spreading Gakkel ridge. Arct. Ocean Nat. 453, 1236–1238. http://dx.doi.org/10.1038/nature07075.

Stanton, T.K., Jezek, K.C., Gow, A.J., 1986. Acoustical reflection and scattering from the underside of laboratory grown sea ice: measurements and predictions. J. Acoust. Soc. Am. 80, 1486–1494.

Wadhams, P., 1980. Oil and ice in the Beaufort Sea–The physical effects of a hypothetical blowout, in Petromar 80: Petroleum and the Marine Environment. Assoc. Eur. Oceanique, Monaco pp. 231–250.

Wadhams, P., Wilkinson, J.P., Kaletzky, A., 2004. Sidescan Sonar Imagery of the Winter Marginal Ice Zone Obtained from an AUV. J. Atmos. Ocean. Technol. 21 (9), 1462–1470.

Wadhams, P., Wilkinson, J.P., McPhail, S.D., 2006. A new view of the underside of Arctic sea ice. Geophys. Res. Lett. 33, L04501. http://dx.doi.org/10.1029/2005GL025131.

Wilkinson, J.P., Wadhams, P., Hughes, N.E., 2007. Modelling the spread of oil under fast sea ice using three-dimensional multibeam sonar data. Geophys. Res. Lett. 34, L22506. http://dx.doi.org/10.1029/2007GL031754.

Williams, K.L., Garrison, G.R., Mourad, P.D., 1992. Experimental examination of growing and newly submerged sea ice including acoustic probing of the skeletal layer. J. Acoust. Soc. Am. 92, 2075–2092.

Williams, G.D., Maksym, T., Wilkinson, J., Kunz, C., Trujillo, E., Steer, A., Kimball, P., Massom, R., Meiners, K.M., Leonard, K., Murphy, C., Heil, P., Lieser, J., Lachlan-Cope, T., Singh, H., 2013. Beyond point measurements: 3-D characterization of sea ice floes. Am. Geophys. Union EOS vol. 94 (No. 7, 12 February).

Yapa, P.D., Chowdhury, T., 1990. Spreading of oil under ice covers. J. Hydraul. Eng. ASCE 1468–1483 (December).

Yapa, P.D., Weerasuriya, S.A., 1997. Spreading of oil spilled under floating broken ice. J. Hydraul. Eng. ASCE 676–683 (August).